Hindawi
Advances in Materials Science and Engineering
Volume 2022, Article ID 9330521, 8 pages
https://doi.org/10.1155/2022/9330521

Research Article

Effect of Shielding Gas on the Microstructure and Properties of Laser-MAG Hybrid Welded Joint for Nickel-Saving Stainless Steel

Naiwen Fang,[1] **Ruisheng Huang**,[1] **Xingxing Wang**,[2] **Jiahao Tian**,[2] **Shuai Li**,[2] **Pengbo Wu**,[1] **Kai Xu**,[1] **Peng He**,[3] **GuoDong Wen**,[4] **and Laizhu Jiang**[5]

[1]*Harbin Welding Institute Limited Company, Harbin 150028, China*
[2]*Henan International Joint Laboratory of High-efficiency Special Green Welding, North China University of Water Resources and Electric Power, Zhengzhou 450045, China*
[3]*State Key Laboratory of Advanced Welding and Joining, Harbin Institute of Technology, Harbin 150001, China*
[4]*Xi'an Research Institute Co. Ltd., China Coal Technology & Industry Group, Xi'an 710077, China*
[5]*Fujian Tsingtuo Special Steel Technology Research Co. Ltd., Ningde 355006, China*

Correspondence should be addressed to Naiwen Fang; naiwen20@163.com and Xingxing Wang; paperwxx@126.com

Received 24 January 2022; Revised 28 February 2022; Accepted 1 March 2022; Published 25 March 2022

Academic Editor: Antonio Riveiro

Laser-MAG (metal active gas) hybrid welding of nickel-saving 08Cr19Mn6Ni3Cu2N stainless steel was carried out by using 98% Ar + 2%N_2 and 95%Ar + 5%CO_2 as shielding gases. The effect of different shielding gases on the microstructure and properties of the welded joints was investigated. The results showed that arc shrinkage was significant with the addition of nitrogen, weld spatter increased with the expansion of arc volume, and arc stability deteriorated. The ferrite content in the weld decreased by about 60%, the ferrite dendrite also gradually became finer, and the secondary dendrite arm was shorter. Only a small amount of δ and γ phases existed in the weld, and no precipitation of the σ phase and nitride was found. Observing four crystal planes, we found that size of the austenite grains decreased with the addition of nitrogen. The average tensile strength of the welded joints decreased from 712 MPa to 704 MPa, but with improved corrosion resistance, the pitting corrosion rate increased from 19.45 g·m^2/h to 18.72 g·m^2/h, and the hardness of weld was slightly reduced.

1. Introduction

Nickel-saving austenitic stainless steel (referred to as nickel-saving steel) is a kind of resource-saving steel with high strength and good toughness. In this type of stainless steel, N instead of the expensive Ni is used as the main austenitizing element [1]. Due to its higher stacking fault energy [2], N which dissolves in steel greatly improves the overall performance of the material while optimizing the material microstructure. In recent years, nickel-saving steel and its welding have received continuous attention in the industry [3–5]. Researchers at home and abroad have conducted numerous investigations on the welding of nickel-saving steel. Zhao et al. [6] used the mixture of nitrogen and argon as shielding gases for TIG welding of low-nickel steel. The behavior of nitrogen and microstructure and mechanical properties of the welded joint obtained were systematically analyzed. Bonnefois et al. [7] used TIG and A-TIG welding processes to join low-nickel steel and found that nitrogen was easy to transit from shielding gas to the molten pool during A-TIG welding. Qiang et al. [8] conducted a double-side coaxial TIG self-fusion welding for low-nickel steel. The study found that with the increase of the proportion of nitrogen in the shielding gas, arc shrinkage was significant, weld spatter increased, and the welding stability deteriorated. To ensure the overall performance of the welded joint, the proportion of nitrogen in the shielding gas shall not exceed 20%. Laser-MAG hybrid welding is a method combining the energy of laser beam and MAG arc. Compared with laser welding or MAG welding separately, the laser-MAG hybrid welding method effectively improves the utilization of arc energy, reduces the loss of laser power, and

increases the stability of arc. The high-energy laser beam can significantly increase weld penetration. Due to the high heat input of its heat resource, hybrid laser-MAG arc welding effectively improves the wettability and spreading performance of metal, improving the weld formation. Also, the hybrid laser-MAG arc welding has features such as concentrated energy density, faster welding speed, smaller heat-affected zone, and lower welding deformation and residual stress. [9–11]. Chen et al. [12] studied the influence of welding angle on weld morphologies, and porosity characteristics were studied in laser arc hybrid welding of AA2219 aluminum (Al) alloy. It was found that the welding process became stable when the transitional position of the droplet was 2 mm away from the keyhole. By analyzing the force acting on the keyhole and characteristics of the pool, it was found that the weld morphologies and porosity characteristics were associated with gravity-laser angle (beta), which affected the keyhole stability and characteristics of the pool. The results showed that the flow velocity was accelerated when the beta value increased, which was good for decreasing porosity. Wang et al. [13] studied the effect of different process parameters, including laser power, energy distribution between the PTA and laser, wire feed speed, travel speed, and laser beam size, on the deposition process, and bead shape was investigated systematically. The results showed that the optimum operating regime for the hybrid process was with the wire being fully melted by the PTA and the melt pool being controlled by the laser, which gave a good bead shape as well as a stable deposition process.

Therefore, it has a broad application prospect in manufacturing field [14, 15]. However, the current relevant research is not sufficient to provide an overview on applying hybrid laser-MAG arc welding for low-nickel steel.

In this study, the low-nickel steel was joined with laser-MAG hybrid welding method, by adjusting the composition of shielding gas. The influence of shielding gas on the microstructure and properties of the welded joints, including the ferrite content and pitting resistance, was analyzed in detail.

2. Experiment Method

The nickel-saving 08Cr19Mn6Ni3Cu2N stainless steel plate with a size of $300 \times 150 \times 12$ mm was used as the base metal for the welding experiment. The filler wire was the same material as the base metal with a diameter of 1.2 mm, and their chemical composition is shown in Table 1.

Figure 1 shows a self-designed hybrid laser-MAG arc welding system, comprised of the KUKA robot, Fronius TPS4000 pulse welding machine, displacement system, and IPG YLS-30000 solid-state laser. Under the mode of continuous laser output, the focus is 460 mm, output wavelength is 1.06 μm, the minimum spot diameter is 0.66 mm, and the maximum output power is 30 kW. Based on previous experimental experience, the optical fiber spacing $d = 6$ mm, laser power is 3.6 kW, and defocusing amount $\Delta f = +18$ mm. A high-speed camera was used to capture the arc shape, and the sampling frequency was 4000 frames/s. In the experiment, the laser front welding method was used. Hybrid laser arc welding was adopted for the welding with two passes. The welding parameters are listed in Table 2. The groove of the test plate to be welded is shown in Figure 2. Before welding, the surface of the experiment plate was polished and the oil stain was removed with acetone. Then, the microstructure of the weld was observed with an optical microscope (OM). The welding arc shape was observed with a PHOTRON ULRM512 high-speed camera. The microhardness of the welded joint was measured with a microhardness tester. The ferrite fraction of the weld was calculated by using FERITSCOPE® FMP30 of German Fisher. The phase composition and content of the weld, as well as the austenite grain size, were measured, and the spot corrosion rate of the joint was tested with XRD.

3. Experiment Results and Discussion

3.1. Effect of Shielding Gas on the Shape of a Welding Arc. Welding arc is the key factor affecting the weld formation, and it was observed by a high-speed camera. Figure 3 shows the arc shape with two kinds of shielding gases. It was found that arc shrinkage was apparent when nitrogen was added to the shielding gas. Figure 3(a) shows that the arc column width decreases with the addition of nitrogen, both spatter and the volume increase, and the arc stability becomes worse, while using $Ar + CO_2$ as the shielding gas, as shown in Figure 3(b), there was almost no spatter during the welding process, and arc shrunk and expanded regularly. When nitrogen was added, the spatter was generated and accompanied by intense smoke because of the low solubility of nitrogen in the liquid molten pool. When the nickel-saving steel was in the melting state, the nitrogen in the external arc atmosphere entered the molten pool in the form of a solute. Then, it overcame the surface tension of the molten pool and broke through the liquid metal to escape. The escaped nitrogen disturbed the atmosphere of the shielding gas, resulting in an unstable arc and uneven arc spray force. Besides, the intervention of the laser increased the attraction to the arc and caused the arc to deflect, which, as a result, caused the increase of arc length [16]. Therefore, the addition of nitrogen increases welding spatter and its volume and results in poor arc stability.

3.2. Effect of Shielding Gas on the Microstructure of Welded Joint. Figure 4 shows the macroprofile of the welded joints with two shielding gases. No welding defects such as porosity, crack, slag inclusion, and incomplete fusion are found on the two welded joints. The weld grain presents columnar shape with the growth direction perpendicular to the fusion line and runs through the weld bead. It can also be seen from the macroprofile of the welded joint that the addition of nitrogen significantly reduces the weld width, which further verifies the view that nitrogen can shrink the arc, reduce the surface driving force of the weld pool, and decrease the width of the arc column.

Figures 5 and 6 show the microstructure of the welded joint with two kinds of shielding gases. It can be seen that the microstructure characteristics of the weld are the same, both

Table 1: Chemical compositions of base metal and filler metal (mass fraction, %).

Type	C	Si	Mn	P	S	Cr	Ni	Mo	Cu	N	V	Nb
08Cr19Mn6Ni3Cu2N	0.071	0.40	6.60	0.040	0.001	18.20	2.90	0.11	1.80	0.245	0.125	0.01

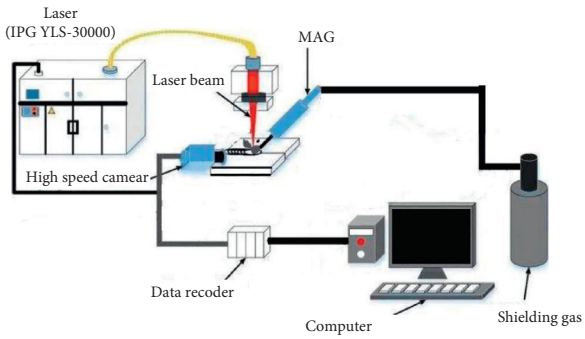

Figure 1: Schematic of hybrid laser-pulse MAG welding system.

Table 2: Welding parameters.

No.	Shielding gas	Gas flow Q (L·min^{-1})	Welding wire feeding speed v_2(m·min^{-1})	Welding current I (A)	Arc voltage U (V)	Welding speed v_1 (mm·s^{-1})	Wire extension l (mm)	Welding gun angle a (°)	Laser incident θ (°)	Distance between laser and arc D (mm)
1	98% Ar + 2%N_2	20	6	200	29	7.5	15	45	8	4
2	95% Ar + 5% CO_2									

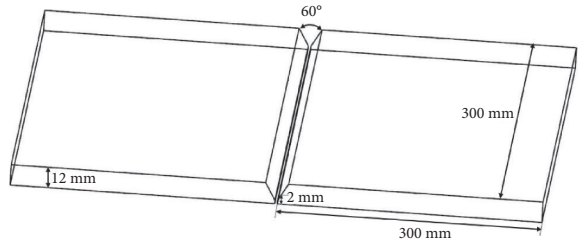

Figure 2: Schematic diagram of prewelding test plate preparation.

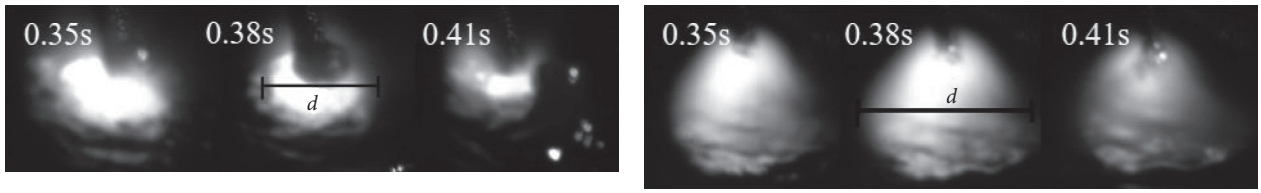

(a) (b)

Figure 3: Arc shape with different shielding gases. (a) 98%Ar + 2%N_2. (b) 95%Ar + 5%CO_2.

composed of an austenite matrix and ferrite dispersed therein. However, in Figure 5(a), the ferrite is skeletally distributed on the austenite dendrite axis with a ferrite content of 3.2%. In Figure 6(a), the ferrite in the weld is vermicular and adheres to the austenite dendrite, and the ferrite fraction, about 8.1%, is relatively high.

The addition of nitrogen makes the ferrite dendrites in the joint thinner and the secondary dendrite arms shorter. During the transformation process from ferrite to austenite + ferrite, the rapid cooling after welding leads to the inability of ferrite to be fully transformed into austenite. At the same time, nitrogen, as a strong element

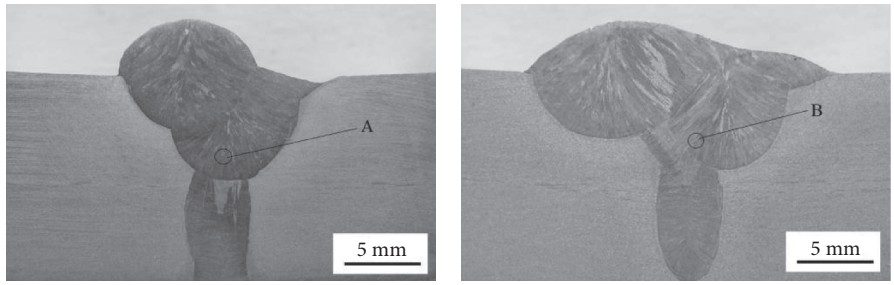

(a) (b)

Figure 4: Macroprofile of the welded joints. (a) 98%Ar + 2%N_2. (b) 95%Ar + 5%CO_2.

(a) (b) (c)

Figure 5: Microstructure of welded joint with shielding gas of 98%Ar + 2%N_2. (a) Weld zone. (b) Fusion zone. (c) Overheating zone.

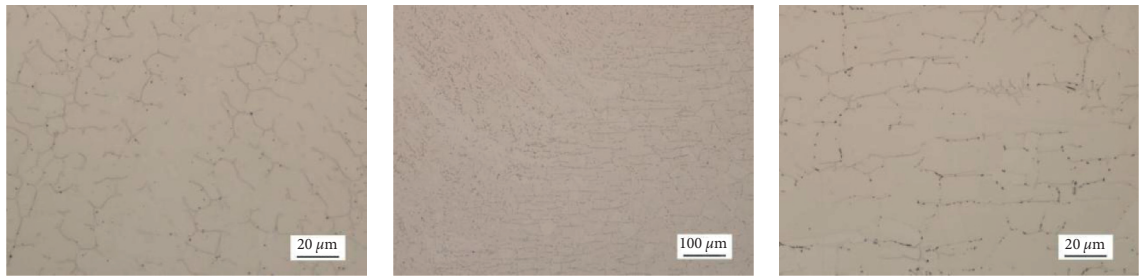

(a) (b) (c)

Figure 6: Microstructure of welded joint with shielding gas of 95%Ar + 5%CO_2. (a). Weld zone. (b) Fusion zone. (c) Overheating zone.

to stabilize austenite, intervenes in the phase transformation process to promote the transformation of austenite during the solidification process, effectively increasing the austenite proportion in the welded joint. Nitrogen is a strong element with a significant role in fine-grain strengthening.

According to the metallographic determination of the structure in the overheating zone in Figure 5(c) and Figure 6(c), the addition of nitrogen refines the grain size from 48.3 μm to 41.1 μm.

Figure 7 shows the ferrite fraction of the joint obtained with different shielding gases by using the ferrite fraction meter. The content trend is consistent with that measured by the metallographic method. The average ferrite content in the weld was reduced from 6.9% to 2.9% after adding nitrogen to the shielding gas.

3.3. Indentation Curve Analysis. The nanoindentation experiments were carried out on the center of the weld zone (point A in Figure 4(a) and point B in Figure 4(b), respectively) of the welded joints with two kinds of shielding gases. From the contact force-indentation depth curve shown in Figure 8, it is found that in the loading stage, the contact force of weld obtained with 98%Ar + 2%N_2 shielding gas is 4600 mN with an indentation depth of 190 nm, while that of the weld with 95%Ar + 5%CO_2 shielding gas is 4999 mN with an indentation depth of 184 nm. In the unloading stage, there is a certain degree of elastic recovery of the indentation depth of the two welds. The weld with shielding gas of 98%Ar + 2% N_2 has a significant degree of recovery, indicating its high elastic modulus.

With the addition of nitrogen into the shielding gas, the average microhardness of the weld decreased. As analyzed

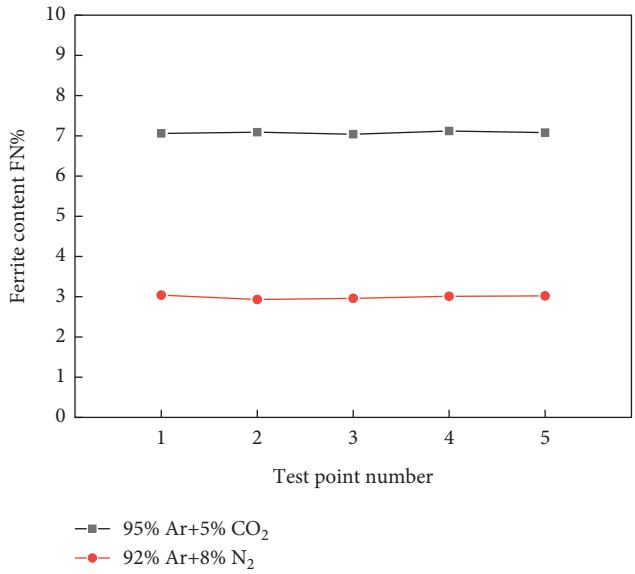

Figure 7: Ferrite content in the weld.

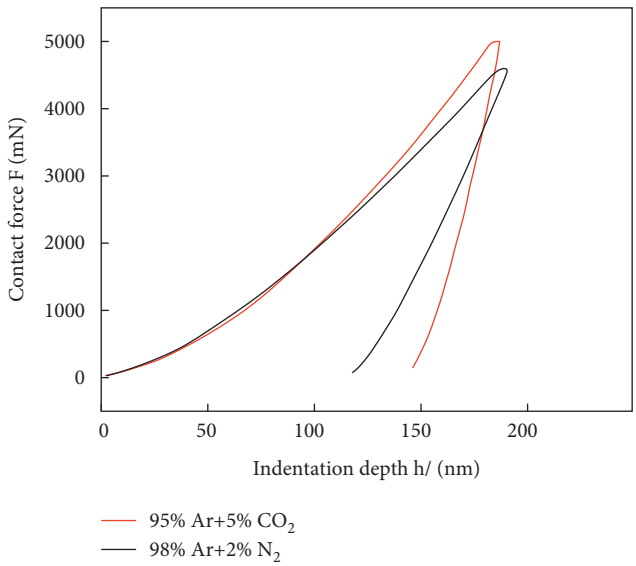

Figure 8: Load-displacement curve.

above, the addition of nitrogen reduced the ferrite content. It increased the austenite content, while the hardness of ferrite was generally lower than that of austenite, resulting in a decrease of the average hardness of the weld structure. Relevant research [17] shows that δ ferrite in the weld can effectively hinder the growth of the austenite structure during the weld solidification process. It has a strong effect on nucleation, which helps to refine the second sub-austenite. The decrease of ferrite content directly affects its effect of hindering the growth of austenite structure and also weakens its nucleation effect.

3.4. X-Ray Diffraction Analysis. Harmful phases such as σ phase and Cr_2N are easy to precipitate in the welding process of low-nickel nitrogen-containing stainless steel, which might seriously damage the mechanical properties and corrosion resistance of the weld structure. XRD analysis was carried out on the weld structure with the two kinds of shielding gases. In Figure 9, there are only a few δ and γ phases in the weld structure, and no precipitation of σ phase, Cr_2N, and Fe_4N is found. It is believed that in the process of hybrid laser arc welding, the metal vapor partial pressure in laser-plasma effectively shares the nitrogen partial pressure in the shielding gas, which results in the low solubility of nitrogen in the molten pool. At the same time, the cooling speed of hybrid laser arc welding joint is very fast, so decomposed N is not able to fully dissolve while the molten pool had already begun to solidify, which also effectively reduces the supersaturated solution of nitrogen in the weld and thus reduces the precipitation of nitride. It can also be found from Figure 9 that the ferrite content decreases due to the addition of nitrogen in the shielding gas, further verifying the measured results with the metallographic method and the ferrite content determination method.

It can be seen from Figure 10 that the addition of nitrogen reduces the austenite grain size on all four crystal planes. N reduces the diffusion coefficient of Cr in austenite, slows down the diffusion of Cr, reduces the lattice constant of carbide, and increases the dislocation of the interface, which weakens the growth power of each phase, thus hindering its nucleation and growth. The measured result is slightly different from that obtained by metallography, but basically, the trend with the two methods is consistent, with ferrite content decreasing about 60%.

3.5. Analysis of Tensile Properties. In austenitic-ferritic stainless steel, because of different physical properties between the austenite phase of FCC structure and the ferrite phase of BCC structure, their interaction generates microstress to maintain the balance between grains of different orientation. Such stress has a significant effect on the stress corrosion cracking and yield behavior of materials, affecting their strength directly. Results show that the decrease in the ferrite mass fraction not only causes a decrease in the strength of the material [18] but also leads to an increase in the weld residual stress [19], which is unfavorable for the strength of the welded joints. Ferrite can effectively hinder the growth of the austenite structure during the weld solidification process. δ ferrite has a strong effect on nucleation, which helps to refine the second sub-austenite. The addition of nitrogen to the shielding gas reduces the mass fraction of ferrite. It weakens the effect of hindering the growth of primary austenite structure and refining secondary austenite structure, leading to the coarsening of austenite structure in the weld and the decrease of the strength of the welded joint. The results of the experiment are shown in Table 3.

3.6. Analysis of Pitting Resistance. Figure 11 shows the macromorphology of the sample after pitting. Pitting most probably occurs in the fusion zone and the base metal, while it seldom appears in the weld. It can be seen from Table 4 that the addition of nitrogen to the shielding gas

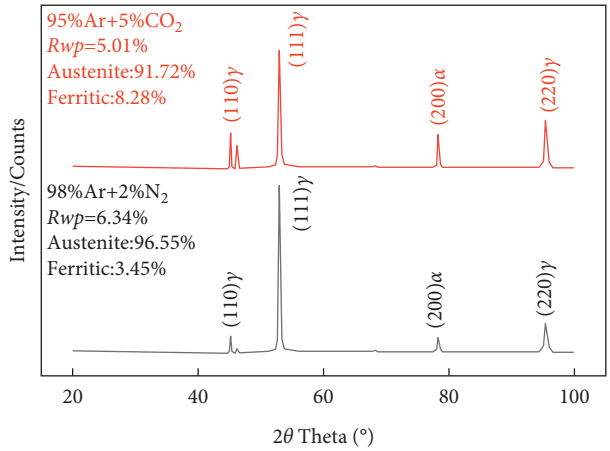

Figure 9: XRD results in weld.

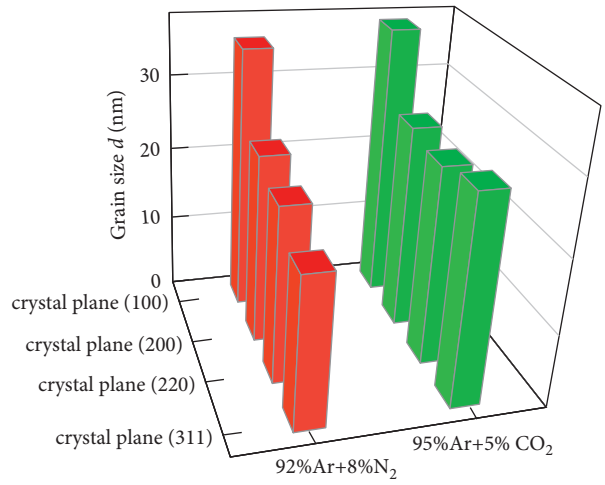

Figure 10: Test results of austenite grain size.

Table 3: Mechanical properties of welded joints.

Shielding gas	Tensile strength R_m (MPa)
92%Ar + 8%N_2	703, 705
95%Ar + 5%CO_2	714, 710

Table 4: Spot corrosion rate of welded joint.

Shielding gas	Length L (mm)	Width W (mm)	Thickness δ (mm)	Initial weight M_1 (g)	Final weight M_2 (g)	Corrosion rate V ($g \cdot m^2 \cdot h^{-1}$)
98%Ar + 2%N_2	44.32	8.00	4.80	13.2071	12.6628	18.72
95%Ar + 5% CO_2	41.88	8.00	5.00	13.1462	12.6005	19.45

slows the pitting speed in the welded joints, indicating that the addition of nitrogen in shielding gas improves the pitting resistance of welded joints. In the welding process, the addition of a certain proportion of nitrogen to the shielding gas promotes the absorption of nitrogen in the welded joint, to make up for the burning loss of nitrogen. Xin et al. [20] suggested that nitrogen mainly existed in austenite structure, which promoted the transfer of chromium and molybdenum in the ferrite to the austenite during the welding melting process, thereby increasing the pitting potential in the austenite structure. Meanwhile, nitrogen is an austenitizing forming element, which steadily expands the austenite phase area. The diffusion coefficient of nitrogen in austenite is higher than that of C, P, Si, and other elements, so nitrogen will preferentially segregate near the grain boundary in the precipitation

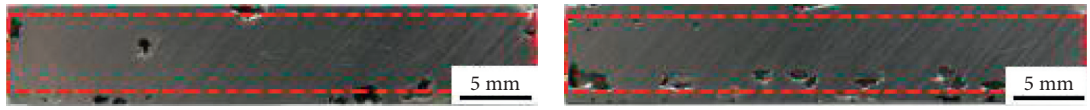

(a) (b)

Figure 11: Macromorphology of pitting specimen. (a) 98%Ar + 2%N_2. (b) 95%Ar + 5%CO_2.

process, slowing down or even inhibiting the precipitation of chromium carbide, thus improving the pitting resistance of 08Cr19Mn6Ni3Cu2N welded joint.

4. Conclusions

Laser-MAG hybrid welding of nickel-saving 08Cr19Mn6Ni3Cu2N stainless steel was carried out by using two kinds of shielding gases. The effect of different shielding gases on the microstructure and properties of the welded joint was investigated. The main conclusions are drawn as follows:

(1) When nitrogen was added into the shielding gas, arc shrunk, both spatter and its volume increased, and arc stability deteriorated. When Ar + CO_2 were used as shielding gas, there was almost no spatter in the welding process, and the arc contracted and expanded regularly. Also, laser intervention increased the attraction to the arc and made the arc deflect, resulting in an increase of the arc length.

(2) By adding nitrogen to the shielding gas, the ferrite in the weld structure was distributed on the austenite dendrite axis as a skeleton. In the weld structure, without adding nitrogen to the shielding gas, the ferrite in the weld was vermicular and adhered to the austenite dendrite. The content of ferrite was relatively high. With the addition of nitrogen, the ferrite dendrite in the weld structure became finer, and the ferrite content decreased by about 60%. The secondary dendrite arm became shorter, and the grain size refined from 48.3 μm to 41.1 μm.

(3) When nitrogen was added into the shielding gas, the average microhardness of the weld slightly decreased. The contact force of weld obtained with 98% Ar + 2%N_2 shielding gas was 4600 mN with an indentation depth of 190 nm, while that of the weld with 95%Ar + 5%CO_2 shielding gas was 4999 mN with an indentation depth of 184 nm.

(4) The addition of nitrogen to the shielding gas reduced the mass fraction of ferrite. The average tensile strength of welded joint decreased from 712 MPa to 704 MPa.

(5) There were only a few δ and γ phases in the weld structure, and no precipitation of σ phase, Cr_2N, and Fe_4N was found. The addition of nitrogen in the shielding gas reduced the austenite grain size on the four crystal planes.

(6) Pitting most probably occurred in the fusion zone and the base metal, while it seldom appeared in the weld. The addition of nitrogen to the shielding gas slowed the pitting speed in the welded joints, from 19.45 g m^2 h^{-1} to 18.72 g m^2 h^{-1}.

Data Availability

The data used to support the findings of this study are included within the article.

Conflicts of Interest

The authors declare that they have no conflicts of interest.

Acknowledgments

This study was supported by the National Natural Science Foundation of China (grant no. 52071165), Natural Science Foundation Excellent Youth Project of Henan (grant no. 202300410268), Program for Science & Technology Innovation Talents in Universities of Henan Province (grant no. 22HASTIT026), China Postdoctoral Science Foundation (project no. 2019M662011), Open Fund of State Key Laboratory of Advanced Brazing Filler Metals and Technology (project no. SKLABFMT201901), and Open Fund of State Key Laboratory of Advanced Welding and Joining (project no. AWJ-21M11). The authors are grateful for the support.

References

[1] H. Dai, X. W. Xia, N. W. Fang, and J. Chang, "Effect of the heat input on microstructure and properties of submerged arc welded joint of low nickel 08Cr19MnNi3Cu2N stainless steel," *China Welding*, vol. 28, no. 3, pp. 48–53, 2019.

[2] Z. Ming, K. H. Wang, W. Fang, and Y. Wang, "Effects of nitrogen content and welding current on Microstructure and properties of the weld of high nitrogen austenite steel," *Transactions of the China Welding Institute*, vol. 40, no. 1, pp. 104–108, 2019.

[3] R. Grzegorz, S. Aleksandra, L. Michał, and F. Dariusz, "Mechanical and microstructural characterization of TIG welded dissimilar joints between 304L austenitic stainless steel and incoloy 800HT nickel alloy," *Metals*, vol. 10, p. 559, 2020.

[4] P. Krzysztof, S. Aleksandra, H. Paulina, and T. Marek, "Laser dissimilar welding of AISI 430F and AISI 304 stainless steels," *Materials*, vol. 13, p. 4540, 2020.

[5] J. Rafał and P. Krzysztof, "Laser welding of austenitic ferrofluid container for the KRAKsat satellite," *Welding in the World*, vol. 65, no. 7, pp. 1347–1357, 2021.

[6] L. Zhao, Z. Tian, and Y. Peng, "Porosity and nitrogen content of weld metal in laser welding of high nitrogen austenitic stainless steel," *ISIJ International*, vol. 47, no. 12, pp. 1772–1775, 2007.

[7] B. Bonnefois, L. Coudreuse, and J. Charles, "A-TIG welding of high nitrogen alloyed stainless steels: a metallurgically high-performance welding process," *Welding International*, vol. 18, no. 3, pp. 208–212, 2004.

[8] W. Qiang, K. H. Wang, and Y. Hou, "Effect of N_2 ratio in shielding gas on welding process characteristic in double-sided coaxial TIG welding of high nitrogen steel," *Transactions of the China Welding Institute*, vol. 38, no. 9, pp. 70–74, 2017.

[9] C. Bagger and F. O. Olsen, "Review of laser hybrid welding," *Journal of Laser Applications*, vol. 17, no. 1, pp. 2–14, 2005.

[10] E. Le Guen, R. Fabbro, M. Carin, F. Coste, and P. Le Masson, "Analysis of hybrid Nd:Yag laser-MAG arc welding processes," *Optics & Laser Technology & Laser Technology*, vol. 43, no. 7, pp. 1155–1166, 2011.

[11] C. Walz, T. Seefeld, and G. Sepold, "Seam geometry and process stability during laser-MIG welding," *Laseropto*, vol. 33, no. 2, pp. 64–72, 2001.

[12] C. Chen, Y. Shen, M. Gao, and X. Zeng, "Influence of welding angle on the weld morphology and porosity in laser-arc hybrid welding of AA2219 aluminum alloy," *Welding in the World*, vol. 64, no. 1, pp. 37–45, 2020.

[13] C. Wang, W. Suder, J. Ding, and S. Williams, "Bead shape control in wire based plasma arc and laser hybrid additive manufacture of Ti-6Al-4V," *Journal of Manufacturing Processes*, vol. 68, pp. 1849–1859, 2021.

[14] L. J. Zhang, J. X. Zhang, A. Gumenyuk, M. Rethmeier, and S. J. Na, "Numerical simulation of full penetration laser welding of thick steel plate with high power high brightness laser," *Journal of Materials Processing Technology*, vol. 214, no. 8, pp. 1710–1720, 2014.

[15] Y. B. Chen, J. Chen, L. Q. Li, and W. Lin, "Properties of arc and weld in laser-TIG hybrid process," *Transactions of the China Welding Institute*, vol. 11, no. 6, pp. 663–673, 2011.

[16] A. Boustheen, F. G. A. Homburg, M. G. A. M. Somhorst, and A. Dietzel, "A layered modular polymeric μ-valve suitable for lab-on-foil: design, fabrication, and characterization," *Microfluidics and Nanofluidics*, vol. 11, no. 6, pp. 663–673, 2011.

[17] B. Deng, Y. Peng, and P. B. Liao, "Effect of nitrogen on the mechanical properties of weld metal of 316L austenitic stainless steel," *Journal of Mechanical Engineering*, vol. 47, no. 18, pp. 66–71, 2011.

[18] D. N. Deepashri and V. S. Raja, "Effect of nitrogen addition on the microstructure and mechanical behavior of 317L and 904L austenitic stainless-steel welds," *Journal of Materials*, vol. 41, no. 7, pp. 2097–2112, 2006.

[19] C. Y. Lin and P. Y. Chen, "Effect of nitrogen content and retained ferrite on the residual stress in austenitic stainless-steel weldments," *Materials Science and Engineering*, vol. 307, no. 12, pp. 165–171, 2001.

[20] G. Xin, X. Q. Wu, Z. N. Zhao, and E. Han, "Characterization of oxide films grown on 316L stainless steel exposed to H_2O_2-containing supercritial water," *The Journal of Supercritical Fluids*, vol. 42, no. 8, pp. 157–164, 2007.